Journal of Environmental Radioactivity 212: 106124 (2020)

A study on a $^{210}Pb_{ex}$ accumulation-decay model for dating moraine soils to trace glacier retreat time

Jiacun Chen[1,3], Xinbao Zhang[1], Ana Navas[2]*, Anbang Wen[1], Xiaoxiao Wang[1], Runchuan Zhang[1]

1 *Key Laboratory of Mountain Surface Processes and Ecological Regulation, Institute of Mountain Hazards and Environment, Chinese Academy of Sciences, Chengdu 610041, China*

2 *Estación Experimental de Aula Dei, Spanish National Research Council (EEAD-CSIC), Avda. Montañana 1005, Zaragoza, 50059, Spain.*

3 *University of Chinese Academy of Sciences, Beijing 100049, China.*

*Corresponding author: anavas@eead.csic.es

Abstract: This paper reports work exploring the potential for using the natural fallout radionuclide $^{210}Pb_{ex}$ to date moraine soils for tracing glacier retreat. Based on the physical processes of $^{210}Pb_{ex}$ deposition, decay and losses due to runoff, a $^{210}Pb_{ex}$ accumulation-decay model ($A_n = I\left[\frac{1-\lambda^{n+1}}{1-\lambda} - \frac{b(c^{n+1}-\lambda^{n+1})}{c-\lambda}\right]$) was developed, where A_n= $^{210}Pb_{ex}$ inventory (Bq·m^{-2}); I = annual inventory of $^{210}Pb_{ex}$ deposition (Bq·m^{-2}); λ = ^{210}Pb decay coefficient (0.969); n = time span (years); b and c = $^{210}Pb_{ex}$ loss coefficients for the runoff pathway. Furthermore, ^{137}Cs was used to identify the ages of the study sites and to support the $^{210}Pb_{ex}$ model results. The model was validated with data obtained from the Hailuogou Glacier Valley, Mt. Gongga, in 2016, where nine glacier retreat moraine points were recorded from 1910–1990 along a retreat length of 1750 m in the valley. $^{210}Pb_{ex}$ inventories increased from 3,669.6 ± 218.5 $Bq·m^{-2}$ at the site where the glacier retreated in 1990 to 10,718.9 ± 167.4 $Bq·m^{-2}$ in 1910. The coefficients of b = 0.6006 and c = 0.9764 were derived from the $^{210}Pb_{ex}$ inventories at the nine sites with recorded glacier retreat times that were marked with special stone and terrain features. The goodness-of-fit (GOF) for the model predictions of glacier retreat times is 65.5%. The results obtained confirm that the fallout radionuclide $^{210}Pb_{ex}$ has potential for dating moraine soils in other cryosphere regions throughout the world as well as for other types of records forming sedimentary landform sequences such as soils on debris flows and alluvial fans.

Keywords: $^{210}Pb_{ex}$ accumulation-decay model, ^{137}Cs, dating moraine soils, glacier retreat time, Hailuogou Glacier, China.

1 INTRODUCTION

Owing to global warming, most glaciers in remote polar and high mountain regions of the world have retreated rapidly, particularly over the past 100 years, but only some glaciers have observational retreat data (Barry, 2006). There is an urgent need for information on recent changes in glacier retreat speeds for assessing the impacts of climate change and its effects on soil and water resources in polar and mountainous regions (Lizaga et al., 2019a). Such information will improve understanding of the impact of climate change on fragile polar and high mountain ecosystems at local and global scales, thereby permitting better management and conservation of soil and water resources (Lopez-Moreno et al., 2016).

Fallout radionuclides (FRN), such as ^{137}Cs and $^{210}Pb_{ex}$, have been widely used for assessing soil loss (Walling et al., 2002; Navas et al., 2013; Chen et al., 2019), tracing sediment sources (Collins et al., 2017; Palazón et al., 2015; Gaspar et al., 2019; Lizaga et al., 2019b), establishing sediment budgets (Navas et al., 2014; Walling et al., 2014) and dating ice and sediment deposits (Morellón et al., 2011). ^{210}Pb is an environmental isotope of the ^{238}U decay series with a half-life of 22.6 years, which is derived from the decay of ^{222}Rn (half-life of 3.8 days). ^{222}Rn is a decay product of ^{226}Ra (half-life of 1622 years) and is widely found in natural soils and rocks. Following ^{226}Ra decay to gaseous ^{222}Rn, part of the resultant ^{222}Rn decays to form ^{210}Pb in soils and rocks. Another small part of ^{222}Rn enters the atmosphere, decays into ^{210}Pb in the atmosphere, and is then contained in fallout back to the surface of the soil in association with precipitation. This fallout is eventually absorbed by the surface soil, and it is this component of the total ^{210}Pb derived from atmospheric fallout that is termed unsupported or excess ^{210}Pb (Robbins, 1978). The deposition of fallout ^{210}Pb from the atmosphere has been relatively constant over time because of its natural origin. This is different from the deposition of ^{137}Cs which is characterised by peak fallout rates in 1963, which subsequently declined to very low values by 1972 in the northern hemisphere as a result of the ban on atmospheric testing of thermonuclear weapons (Larsen, 1985). The Chernobyl accident increased soil radioactivity levels in the northern hemisphere, especially in eastern Europe, but negligible activities of Chernobyl ^{137}Cs fallout were detected in China in 1986 (Zhang, 2005).

$^{210}Pb_{ex}$ is commonly applied to assess soil redistribution (Gaspar et al., 2013; Porto et al., 2018), but the radionuclide is also used for dating sediment records retrieved from water bodies to reconstruct dynamic changes in sediment accumulation (Morellón et al., 2011). Source models comprised of a number of requirements related to the fallout rate of the radionuclide or the constant accumulation of sediments have been developed (Appleby & Oldfield, 1978). For example, the constant initial concentration (CIC) model (Krishnaswamy et al., 1971) was applicable when the amount of $^{210}Pb_{ex}$ carried and captured by sediments per unit mass was constant and the deposition rate was constant. The constant rate of supply (CRS) model assumes that $^{210}Pb_{ex}$ flux is constant and accumulation rate varies with time, the flux of $^{210}Pb_{ex}$ entering the interface between atmosphere and water is dynamically balanced with its flux entering the interface between water and sediment (Sanchez-Cabeza et al., 2000). Other models were specifically developed to date fluvial deposits with $^{210}Pb_{ex}$ considering the continuous sedimentation occurring in floodplains (He & Walling, 1996).

For regions where lakes are nonexistent, there is a need to find alternative sedimentary deposits that can fulfill suitable stability conditions so as to develop a deposition model fulfilling the conditions for reconstructing the chronology of the sediment deposition. Special conditions in the Hailuogou Valley located at the foot of the Tibetan Plateau have prevented the preservation of lakes and therefore sedimentary records deposited at their bottoms from which to reconstruct the recent history of sediment accumulation generated after glacier retreat are absent.

In light of the situation described above, this study explored the potential for using $^{210}Pb_{ex}$ to date moraine soils and trace glacier retreat over the past 100 years. Based on the physical processes of $^{210}Pb_{ex}$ deposition, losses with runoff that remove fine particles where $^{210}Pb_{ex}$ is fixed and decays, a preliminary $^{210}Pb_{ex}$ accumulation-decay model was developed. The model also considered the change of erosion rate, especially water erosion (Berhe et al., 2018; Liu et al., 2019), which decreased with vegetation growth in the valley following the glacier retreat. To this aim, a field campaign was undertaken in the Hailuogou Glacier Valley in 2016 at Mt. Gongga (Hengduan Range, China) a benchmark site of the IAEA INT5153 Project, “Assessing the Impact of Climate Change and its Effects on Soil and Water Resources in Polar and Mountainous Regions.” Following the direction of glacier retreat along the valley, nine sampling sites were selected based on the known chronology of moraine deposits. The precise moraine position was marked by boundary stones at each site over the period from 1910 to 1990 (Luo et al., 2015). Furthermore, fallout of ^{137}Cs was used to identify the ages of the study sites, labeled by the ^{137}Cs peak in 1963 and to assess if soil mobilization by water erosion occurred at the study sites. In addition, ^{137}Cs was used to support the $^{210}Pb_{ex}$ model results. The model was validated using these recorded retreat times and combining the data on $^{210}Pb_{ex}$ inventories with the time spans between the glacier retreat year and the sampling year for the moraine soil at the nine measurement points.

2 MATERIALS AND METHODS

2.1 Study Area

This study was carried out in the glacier retreat area of Hailuogou Valley in Mt. Gongga, which is located in the Ganzi Tibetan Autonomous Prefecture of Sichuan Province, China (Figure 1). Mt. Gongga is situated in the middle of the Hengduan Mountain range, which is located on the southeastern edge of the Tibet Plateau. The peak of Mt. Gongga is 7553 m asl and its snow line elevation varies between 4800–5200 m. Glaciers on Mt. Gongga have a total area of 255.1 km^2 with a total volume of ~24.65 km^3; the largest one, the Hailuogou Glacier, has a length of 13.1 km and a corresponding area of 25.71 km^2. The annual mean temperature at 3000 m on Mt. Gongga was 4.2°C since 1988, but in the past two decades, the temperature has increased 0.35°C/decade at the Hailuogou Weather Station (Wu et al., 2013). The glacier in Hailuogou valley retreated from 2830 m asl in 1936 to 3000 m asl in 2006 with a retreat length of 1.15 km and an average retreat speed of 19.6 m/year during the period 1990–2004. The annual runoff yield of the Hailuogou ravine increased by 12.9% per year from $232.4 \times 10^6\ m^3$ (1994) to $684.5 \times 10^6\ m^3$ (2005). The average annual precipitation is 1,974 mm (Liu et al., 2010). The valley floor is flat and the river channel incises the valley floor leaving the moraine deposits in the valley largely unaffected by floods. Since the end of the Little Ice Age (LIA, from mid-seventeenth to early eighteenth century), the Hailuogou Glacier retreated markedly with the rising of global temperature, producing a moraine channel and side moraine. Soil and vegetation gradually developed on the exposed glacier soil (Zhou et al., 2013).

Consequently, a typical soil chronological sequence and a complete primary vegetation succession sequence have developed in the Hailuogou Glacier retreat area. The native succession sequence of soil and vegetation is about 2 km long from the end of the glacier that exists integrally and continuously on moraine deposits with big boulders and sandy sediments. At the end of the glacier, there is fresh bare sandy sediment soil in micro-depressions surrounded by big boulders. As seen in the photographs (Fig. 1) the soil gradually evolves to be brown soil with dark colour and high content of organic matter along the transition from bare land to mature subalpine conifer forests. The vegetation succession is: bare ground of moraine grass such as *Astragalus mongholicus* (1990s), young alder and willow, *Hippophae rhamnoides* (1980s), medium alder and willow (1970s), young *Picea-Abies* alder (1960s), *Picea-Abies* (1940s) and *Picea-Abies* (1930s). After 125 years, the biomass and productivity of the plant community is very high (Luo et al., 2017). The position of the glacier tongue during glacier retreat and the vegetation succession at nine selected sites were accurately recorded by researchers at the Experimental Station of Mt. Gongga, using the existing stone marks and analysing terrain features and vegetation changes along the glacier valley (Luo et al., 2012; Zhou et al., 2016).

2.2 Field Sampling and Laboratory Analysis

Sampling was carried out in May of 2016. Nine appropriate flat or micro-depression and undisturbed sites (R1–R9) were carefully selected for sampling soil profiles. The glacier retreat time at each site along the Hailougou Valley is well documented from 1910–1990 (Table 1).

At each site, a square sampling section (50 x 50 cm) was established. The section was excavated from the top surface down to a depth of 10 cm to extract 1 cm samples at regular intervals. At each site, 10 stratified samples were obtained totaling 90 depth interval samples collected from the nine study sites (R1 to R9).

Prior to analysis, all samples were air dried, disaggregated, passed through a 2 mm sieve, homogenised and sealed hermetically into cylindrical containers for ≥21 days to achieve equilibrium between ^{226}Ra and its daughters. The activities of ^{210}Pb, ^{226}Ra and ^{137}Cs were measured in the isotope laboratory of the Chengdu Institute of Mountain Hazards and Environment at the Chinese Academy of Sciences. The activities of $^{210}Pb_{ex}$ and ^{137}Cs in the samples were measured by gamma spectrometry, using a high resolution, low background, low energy and hyper-pure *n*-type LOAX HPGe detector (ORTEC, Oak Ridge, Tennessee, USA). Each sample weighed ≥500 g and counting times were in excess of 80,000 s, providing a precision of approximately ±10% at the 90% level of confidence for the gamma ray measurements. ^{137}Cs was detected at 662 keV. The total ^{210}Pb activity was obtained using the 46.5 keV gamma ray from ^{210}Pb and ^{226}Ra concentrations were obtained using the 351.9 keV gamma ray from ^{214}Pb, a short-lived daughter of ^{226}Ra. Unsupported ^{210}Pb ($^{210}Pb_{ex}$) concentrations in the samples were calculated by subtracting the ^{226}Ra-supported ^{210}Pb concentrations from the total ^{210}Pb concentrations. The grain size distributions (sand, silt and clay sizes) of the samples were measured using a laser-diffraction granulometer (Mastersizer 2000, Malvern, UK); in this case, the samples were successively pretreated with 10% H_2O_2 and 10% HCl to remove organic matter and

$CaCO_3$, respectively (Shi, et al. 2017). All samples were dispersed using an ultrasonic probe for one minute before the measurements for absolute grain size distributions were made.

3 RESULTS

3.1 Particle size composition

The particle size depth distributions of the moraine soils are shown in Figure 2. The average proportions of clay (<2μm) ranged between 0.19–0.97% with a corresponding mean of 0.31%, silt (2–63 μm) between 26.64% and 61.33% with a mean of 44.49% and sand (63–2000 μm) between 38.46% and 73.29% with a mean of 55.2%. The mean median diameter (d_{50}) of the nine moraine sites ranged between 44–113 μm with a mean value of 77 μm. The silt content in the recent moraine sites (R1 and R2) was lower than that of the older moraine soils at sites R6 through R8 which were covered with dense vegetation. The silt content decreased with depth in the mature moraine soil at R9. The clay content was very low in all profiles except at R6, mainly because the moraine soil was in the early stages of development.

3.2 Distribution of ^{137}Cs and $^{210}Pb_{ex}$

Little ^{137}Cs was detected in recent soils at R1 (1990) and R2 (1983), which contain ^{137}Cs transported with the sediments, while almost no ^{137}Cs was found at R4 (1966) because the moraine deposit was formed shortly after the 1963 ^{137}Cs peak. However, the older moraine soils formed before the ^{137}Cs peak at R7 (1930), R8 (1915) and R9 (1910) had the highest ^{137}Cs inventories ranging from 764.7 ± 29.8 $Bq \cdot m^{-2}$ to 891.23 ± 54.3 $Bq \cdot m^{-2}$ (Table 2). The depth distributions of ^{137}Cs (Figure 3) exhibit typical profiles at R7 and R9, where the highest concentrations occurred in the top layers and declined exponentially as depth increased. In these profiles, only low levels of ^{137}Cs were detected in the layers below 8 cm depth. Despite the fact that random initial fallout might affect spatial variability of ^{137}Cs inventories (Owens & Walling, 1996), the value of 850.6 $Bq \cdot m^{-2}$, which is the average of two points, was considered to be the local ^{137}Cs reference inventory because it is in agreement with reference inventory values predicted for China by Qi et al. (2006). The ^{137}Cs inventory at R8 was less than that of R7 and R9, and the highest ^{137}Cs concentration occurred in the middle layer at 4–6cm depth, indicating that both erosion and deposition have taken place since 1963 at this site (Figure 3). The ^{137}Cs inventory increased from 105.2 ± 17.4 $Bq \cdot m^{-2}$ at R3 (1972) to 588.2 ± 39.8 $Bq \cdot m^{-2}$ at R6 (1945) and the ^{137}Cs depth distribution curves gradually became typical, because little ^{137}Cs was produced by atomic weapon testing after the 1960s (Sutherland, 1991). The ^{137}Cs inventories in soil formed before the ^{137}Cs peak at sites R5, R6 and R8 were lower than the local reference inventory since part of the ^{137}Cs fallout was removed by water erosion (Liu et al., 2018) resulting from rainfall and snow melt (Table 2, Figure3).

The depth distributions for $^{210}Pb_{ex}$ at the nine sites are shown in Figure 4. In general, the $^{210}Pb_{ex}$ depth distribution curves in soils at the nine sites have similar shapes, with the highest concentration of $^{210}Pb_{ex}$ occurring in the top layers, except in the case of R4 and R8, and then declining exponentially as depth increased. Little $^{210}Pb_{ex}$ was detected in the layer below a depth of 8 cm. Despite the fact that little ^{137}Cs was detected in the soil at R1 (1990), there was a considerable amount of $^{210}Pb_{ex}$

with an inventory of 3,669.6 ± 218.5 Bq·m^{-2} at R1 site. Across the sampling sites, the variation of the $^{210}Pb_{ex}$ inventories with time had a similar pattern as ^{137}Cs, increasing with the span of time between the glacier retreat and the sampling year, reaching its highest value of 10,718.9 ± 167.4 Bq·m^{-2} at site R9 (Table 2, Figure5).

4 DISCUSSION

4.1 Temporal variations of ^{137}Cs and ^{210}Pb$_{ex}$ inventories

Since the sources of ^{137}Cs and $^{210}Pb_{ex}$ are different, there is a difference in the total ^{137}Cs and $^{210}Pb_{ex}$ inventory curves at the nine moraine sites on a temporal scale. In general, both radionuclides gradually increased with time. Apart from sites R1–R4 where moraine soils formed after the 1963 ^{137}Cs peak, the inventories of ^{137}Cs at R5 and R6, prior to the ^{137}Cs peak (Owens et al., 1997), were significantly lower than those at R7 and R9 because older sites from R7–R9 experienced increased ^{137}Cs fallout during the nuclear weapon test period and presumably had more dense vegetation cover protecting the soil surface at that time. On the contrary, the increase of $^{210}Pb_{ex}$ inventories without obvious inflection point over the nine moraine sites is attributed to the fallout process of $^{210}Pb_{ex}$, which exhibits a continuous and stable fallout rate on a temporal scale. However, the $^{210}Pb_{ex}$ inventory values at R3 (1972) and R6 (1945) were irregularly lower. This implies that severe erosion occurred during the period of soil and vegetation development since the glacier retreated from these two specific sites likely due to runoff though soil disturbance by wildlife can not be totally discarded.

4.2 Proposal of a new $^{210}Pb_{ex}$ accumulation-decay model

Existing theoretical $^{210}Pb_{ex}$ models make this approach convenient for wider adoption, including for example, the mass balance model for $^{210}Pb_{ex}$-based estimates of soil loss (Walling & He, 1999, 2002), which is based on the physical processes of the fallout redistribution after its deposition on the soil surface. For dating lake deposits, existing models consider both the ^{210}Pb contained in the sediments accumulated in the lake plus the ^{210}Pb atmospheric flux.

However, when lake records are not available the use of other kinds of deposits such as moraine soils can be made. Hence, for recent moraine soils, there is no input of sediments; only that of the atmospheric ^{210}Pb fallout.

Considering this assumption we propose the following accumulation-decay model:

$$A_n = I + \lambda I + \lambda^2 I + \lambda^3 I + \cdots\cdots + \lambda^{n-1} I + \lambda^n I \qquad [1]$$

where: A_n(Bq · m^{-2}) is the $^{210}Pb_{ex}$ inventory after n years since glacier retreat; I (Bq · m^{-2}) is the annual inventory of $^{210}Pb_{ex}$ fallout from the atmosphere; λ is the decay constant of ^{210}Pb (λ= 0.969); n is the time span between the sampling and glacier retreat (in years).

The change in the $^{210}Pb_{ex}$ inventory in soil can be described by equation [1], assuming that the deposited fallout of $^{210}Pb_{ex}$ from the atmosphere is totally absorbed by the soil and that there is no loss with runoff resulting from rainfall or snow melt. The mass balance model is not applicable in situations where the $^{210}Pb_{ex}$ fails to reach a steady state equivalent to four decay periods (around 100 years).

Furthermore, the likely loss of ^{222}Rn by exhalation (Du & Walling, 2012), especially in coarse textured soils has to be considered. Then, assuming equilibrium the supported ^{210}Pb will be less than that estimated from ^{226}Ra. However, as soils develop and became enriched in organic matter, the importance of such an effect would decline with time. In addition, the mass balance places emphasis on changes in the relative magnitude of the inventory over time rather than on its absolute magnitude.

However, under natural conditions, following ^{210}Pb deposition on the ground due to precipitation, part of the $^{210}Pb_{ex}$ fallout is lost through runoff, which transports fine soil particles as well as snow melt. As the development of soil and vegetation continues, the proportion of $^{210}Pb_{ex}$ lost (θ) with runoff will decrease with time, and this can be expressed by the following power-exponential function, describing the shape of the curve presented in Figure 5:

$$\theta_i = bc^i \qquad [2]$$

where, θ is the proportion of $^{210}Pb_{ex}$ lost with runoff; b and c are $^{210}Pb_{ex}$ runoff loss coefficients, respectively, i is the time spans. b is the initial loss coefficient of $^{210}Pb_{ex}$, which is related to the erodibility of moraine soil after glacier retreated, its value is between 0 and 1. For sandy moraine soils without vegetation cover, the stronger the rainfall erosion intensity is, the closer the value b approaches to 1. c is a parameter related to the rate of vegetation restoration, usually between 0.9 and 1. When c is 1, it means that the bare moraine soils have no vegetation restoration over time, the smaller the value of c, the faster the rate of vegetation restoration. In this study area, the simulation value of coefficient c is 0.9764, it means when i is 100 years, the proportion of $^{210}Pb_{ex}$ lost with runoff (θ_{100}) is 0.055.

Considering losses of $^{210}Pb_{ex}$ fallout with runoff transporting fine particles in which $^{210}Pb_{ex}$ is fixed, the accumulation and decay model is described as:

$$A_n = I(1-bc^n) + \lambda I(1-bc^{n-1}) + \lambda^2 I(1-bc^{n-2}) + \cdots + \lambda^{n-1} I(1-bc) + \lambda^n I(1-b) \quad [3]$$

and equation [3] can be re-expressed as:

$$A_n = I\left[\frac{1-\lambda^{n+1}}{1-\lambda} - \frac{b(c^{n+1}-\lambda^{n+1})}{c-\lambda}\right] \quad [4]$$

The application of the model in a region requires independent information on the date of the moraine deposit after glacier retreat, in order to calibrate the model and calculate the coefficients b and c.

4.3 Testing the $^{210}Pb_{ex}$ accumulation-decay model using data from Hailuogou Valley

The R9 site where the glacier retreated in 1910 is covered by dense conifer forests and has well-developed brown soil with a thick layer of litter in the sampling year 2016. It also had the highest $^{210}Pb_{ex}$ inventory of 10,718.9 ± 167.4 Bq·m^{-2} and perfect depth distribution curves. The 106-year time span between when the moraine was deposited and the sampling year is five times that of the ^{210}Pb decay half-life (22.6 years). Therefore, the inventory of 10,718.9 Bq·m^{-2} was taken to represent the reference inventory in the study area and the annual inventory of $^{210}Pb_{ex}$ fallout (I) was derived as 344.5 Bq·m^{-2} on this basis. The $^{210}Pb_{ex}$ runoff loss coefficients b and c can be derived from the annual inventory of $^{210}Pb_{ex}$ fallout (I) and $^{210}Pb_{ex}$ inventories

(A_n) for a number of time spans (n) using the solver tool in Microsoft Excel. The coefficients of b and c were derived as 0.6006 and 0.9764, respectively, from the $^{210}Pb_{ex}$ inventories (A_n) and the time spans (n) for the nine sites. The goodness-of-fit (GOF) model was tested using the calculated relative difference between actual and modelled values (Motha et al., 2003) as in equation [5]:

$$\mathrm{GOF} = \left\{1 - \frac{\sum_1^m\left(\frac{|A_n - A_n'|}{A_n}\right)}{m}\right\} * 100 \qquad [5]$$

where A_n' is the modelled value of $^{210}Pb_{ex}$ inventory and m is the sample size involved in the parametric simulation of the model. In this case, the nine sites generated a GOF of 65.5%. However, by excluding sites R3 and R6, where the $^{210}Pb_{ex}$ inventory values are irregularly low because of severe erosion since the glacier retreated from these sites, the GOF reached 90% with values of the coefficients b and c of 0.6011 and 0.9756, respectively.

These results show the potential for dating moraine deposits after glacier retreat despite some of the moraine deposits deviating from the curve fit, suggesting that more research is needed to improve the adjustment of the model (Table 3, Figure 5).

5 Conclusions

Both ^{137}Cs and $^{210}Pb_{ex}$ fallout inventories in moraine soils increase as time increases due to glacier retreat in the Hailuogou Valley. The $^{210}Pb_{ex}$ inventories increased from 3,669.6 ± 218.5 $Bq \cdot m^{-2}$ at the site where glacier retreated in 1990 to 10,718.9 ± 167.4 $Bq \cdot m^{-2}$ at the site in 1910; however, little ^{137}Cs fallout was detected in the soils where the glacier retreated after the 1960s because of limited nuclear weapon testing in the world since that time. Based on the physical processes of fallout deposition, decay and losses with runoff, a $^{210}Pb_{ex}$ accumulation-decay model was developed for assessing the time of glacier retreat by dating moraine soils over the past 100 years.

The calculated glacier retreat times for seven of the nine sampled sites are in good agreement with actual measured times, thereby showing the potential for using the $^{210}Pb_{ex}$ technique for dating moraine soils in other cryosphere regions. A careful selection of the sampling sites is important for model results and for reproducibility of b and c coefficients, therefore stable soils with no signs of erosion and not receiving runoff from adjacent areas should be selected.

Further research is needed to test the broader applicability of the approach reported here and to validate the model for additional sites including determination of the runoff loss coefficients *b* and *c* under different environmental conditions and settings. A similar approach could be applied to other types of recently developed sedimentary soils forming a landform sequence as in the case of moraines, such as soils on debris flows and alluvial fans that, after their occurrence, stabilise and are not later covered by further sediment deposits.

Acknowledgements

The study reported in this paper was supported by the National Natural Science Foundation of China (41873025) and by the International Atomic Energy Agency (IAEA; program ++). The assistance of the Alpine Ecosystem Observation and

Experiment Station of Mt. Gongga and the Hailuogou Scenic Area Administrative Committee are also gratefully acknowledged.

References

Appleby P G, Oldfield F. 1978. The calculation of lead–210 dates assuming a constant rate of supply of unsupported ^{210}Pb to the sediment. Catena, 5(1):1–8. DOI: 10.1016/S0341-8162(78)80002-2.

Barry R G. 2006. The status of research on glaciers and global glacier recession: A review. Progress in Physical Geography, 30(3):285-306. DOI: 10.1191/0309133306pp478ra.

Berhe AA, Barnes RT, Six J, Marin-Spiotta E. 2018. Role of Soil Erosion in Biogeochemical Cycling of Essential Elements: Carbon, Nitrogen, and Phosphorus. Annual Review of Earth and Planetary Sciences, 46: 521-548. DOI: 10.1146/annurev-earth-082517-010018.

Chen J, Shi Z, Wen A, Yan D, Chen T. 2019. ^{137}Cs-Based Variation of Soil Erosion in Vertical Zones of a Small Catchment in Southwestern China. International Journal of Environmental Research and Public Health, 16(8):1371. DOI: 10.3390/ijerph16081371.

Collins A L, Pulley S, Foster I D, Gellis A, Porto P, Horowitz A J. 2017. Sediment source fingerprinting as an aid to catchment management: A review of the current state of knowledge and a methodological decision-tree for end-users. Journal of Environmental Management, 194:86-108. DOI: 10.1016/j.jenvman.2016.09.075.

Du P, Walling D E. 2012. Using ^{210}Pb measurements to estimate sedimentation rates on river floodplains. Journal of Environmental Radioactivity, 103(1):59-75. DOI: 10.1016/j.jenvrad.2011.- 08.006.Gaspar L, Navas A, Machín J, Walling, DE. 2013. Using $^{210}Pb_{ex}$ measurements to quantify soil redistribution along two complex toposequences in Mediterranean agroecosystems, northern Spain. Soil

& Tillage Research, 130:81-90. DOI: 10.1016/j.still.2013.02.011.

Gaspar L, Navas A. Machín J., Walling, D.E., 2013. Using $^{210}Pb_{ex}$ measurements to quantify soil redistribution along two complex toposequences in Mediterranean agroecosystems, northern Spain. Soil & Tillage Research, 130: 81-90. doi:10.1016/j.still.2013.02.011

Gaspar L, Lizaga I, Blake W H, Latorre B, Quijano L, Navas A. 2019. Fingerprinting changes in source contribution for evaluating soil response during an exceptional rainfall in Spanish Pre-Pyrenees. Journal of Environmental Management, 240:136-148.doi.org/10.1016/j.jenvman.2019.03.109.

He Q and Walling D E. 1996. Use of fallout Pb-210 measurements to investigate longer-term rates and patterns of overbank sediment deposition on the floodplains of lowland rivers. Earth Surface Processes and Landforms, 21(2): 141-154. DOI: 10.1002/(sici)1096-9837(199602)21:2<141::ai-d-esp572>3.0.co;2-9.

Krishnaswamy S, Lal D, Martin J M, et al. 1971. Geochronology of lake sediments. Earth & Planetary Science Letters, 11(1):407-414. DOI: 10.1016/0012-821X(71)90202-0.

Larsen R J. 1985. Worldwide Deposition of ^{90}Sr through 1983. EML-444, Environmental Measurements Laboratory, U.S. Department of Energy, New York, 159.

Liu C, Li Z W, Berhe A A, Xiao H B, Liu L, Wang D Y, Peng H, Zeng G M. 2019. Characterizing dissolved organic matter in eroded sediments from a loess hilly catchment using fluorescence EEM-PARAFAC and UV–Visible absorption: Insights from source identification and carbon cycling. Geoderma, 334: 37-48. DOI: 10.1016/j.geoderma.2018.07.029

Liu C, Li Z W, Chang X F, Nie X D, Liu L, Xiao H B, Wang DY, Peng H, Zeng G M. 2018. Apportioning source of erosion-induced organic matter in the hilly-gully region of loess plateau in China: Insight from lipid biomarker and isotopic signature analysis. Science of the Total Environment, 621: 1310-1319. DOI: 10.1016/j.scitotenv.2017.10.097.

Liu Q, Liu S, Zhang Y, Wang X, Zhang Y, Guo W, Xu J. 2010. Recent shrinkage and hydrological response of Hailuogou glacier, a monsoon temperate glacier on the east slope of Mount Gongga, China. Journal of Glaciology, 56(196):215-224. DOI: 10.3189/002214310791968520.

Lizaga I, Gaspar L, Quijano L, Dercon G, Navas A. 2019a. NDVI, ^{137}Cs and nutrients for tracking soil and vegetation development on glacial landforms in the Lake Parón Catchment (Cordillera Blanca, Peru). Science of the Total Environment, 651:250-260. DOI: 10.1016/j.scitotenv.2018.09.075.

Lizaga, I., Gaspar, L., Blake, W.H., Latorre, B., Navas, A. 2019b. Fingerprinting changes of source apportionments from mixed land uses in stream sediments before and after an exceptional rainstorm event. Geomorphology, 341: 216-229. https://doi.org/10.1016/j.geomorph.2019.05.015

López-Moreno J I, Morán-Tejeda E, Vicente-Serrano S M, Bazo J, Azorin-Molina C, et al. 2016. Recent temperature variability and change in the Altiplano of Bolivia and Peru. International Journal of Climatology, 36(4):1773-1796. DOI: 10.1002/joc.4459.

Luo J, Chen Y, Wu Y, Shi P, Jia S, & Peng Z. 2012. Temporal-Spatial Variation and Controls of Soil Respiration in Different Primary Succession Stages on Glacier Forehead in Gongga Mountain, China. Plos One, 7(8):e42354. DOI: 10.1371/journal.pone.0042354.

Luo J, Tang R, Sun S, Yang D, Jia S, & Yang PJ. 2015. Lead distribution and possible sources along vertical zone spectrum of typical ecosystems in the Gongga Mountain, eastern Tibetan Plateau. Atmospheric Environment, 115:132-140. DOI: 10.1016/j.atmosenv.2015.05.022.

Luo J, Wei L, She J, He Y, Gao, J. 2017. Carbon Dynamics in Different Primary Succession Stages On Hailuogou Glacier Forehead in Mount Gongga, China. Mountain Research, 37(5):629-635. DOI: 10.16089/j.cnki.1008-2786.000261.

Motha J A, Wallbrink P J, Hairsine P B, Grayson R B. 2003. Determining the sources of suspended sediment in a forested catchment in southeastern Australia. Water Resources Research, 39(3):53-62. DOI: 10.1029/2001WR000794.

Morellón M, Valero-Garcés B, González-Sampériz P, Vegas-Vilarrúbia T, Rubio E, et al. 2011. Climate changes and human activities recorded in the sediments of Lake Estanya (NE Spain) during the medieval warm period and little ice age. Journal of Paleolimnology, 46(3):423-452. DOI: 10.1007/s10933-009-9346-3.

Navas A, López-Vicente M, Gaspar L, Machín J. 2013. Assessing soil redistribution in a complex karst catchment using fallout ^{137}Cs and GIS. Geomorphology, 196:231-241. DOI: 10.1016/j.geomorph.2012.03.018.

Navas A, López-Vicente M, Gaspar L, Palazón L, Quijano L. 2014. Establishing a tracer-based sediment budget to preserve wetlands in Mediterranean mountain agroecosystems (NE Spain). Science of the Total Environment, 496: 132-143. DOI: 10.1016/j.scitotenv.2014.07.026

Owens P N, Walling D E. 1996. Spatial Variability of Caesium-137 Inventories at Reference Sites: an Example from Two Contrasting Sites in England and Zimbabwe. Applied Radiation and Isotopes, 47(7): 699-707. DOI: 10.1016/0969-8043(96)00015-2.

Owens P N, Walling D E, He Q, et al. 1997. The use of caesium-137 measurements to establish a sediment budget for the Start catchment, Devon, UK. Hydrological Sciences Journal, 42(3): 405-423. DOI: 10.1080/02626669709492037.

Palazón L, Latorre B, Gaspar L, Blake W H, Smith H G, Navas A. 2015. Comparing catchment sediment fingerprinting procedures using an auto-evaluation approach with virtual sample mixtures. Science of the Total Environment, 532: 456-466. DOI: 10.1016j.scitotenv.2015.05.003.

Porto P, Walling D E, Callegari G. 2018. Using repeated ^{137}Cs and ^{210}Pb$_{ex}$ measurements to establish sediment budgets for different time windows and explore the effect of connectivity on soil erosion rates in a small experimental catchment in Southern Italy. Land Degradation & Development, 29:1819–1832. DOI: 10.1002/ldr.2815.

Qi Y Q, Zhang X B, He X B, Wen A B, Fu J X. 2006. ^{137}Cs reference inventories distribution pattern in China. Nuclear Techniques, 29(1): 42-50. DOI: 10.1111/j.1745-4557.2006.00081.x.

Robbins J. 1978. Geochemical and geophysical applications of radioactive lead. Biogeochemistry of Lead in the Environment, 286–383.

Sanchez-Cabeza J, Ani-Ragolta I, & Masque P. 2000. Some Considerations of the210Pb Constant Rate of Supply (CRS) Dating Model. Limnology and Oceanography, 45(4): 990-995. DOI: 10.2307/2670566.

Sutherland R A. 1991. Examination of caesium-137 areal activities in control (uneroded) locations. Soil Technol, 4: 33-50. DOI: 10.1016/0933-3630(91)90038-O.

Shi Z, Wen A, Walling D E, Wang Y, Chen J. 2017. Exploring particle size selectivity effects during erosion of purple soils in Chongqing municipality, China. Journal of Soils & Sediments, 17(4):1191-1196. DOI: 10.1007/s11629-017-4486-9.

Walling D E, He Q. 1999. Using fallout lead-210 measurements to estimate soil erosion on cultivated land. Soil Science Society of America Journal, 63: 1404-1412. DOI: 10.2136/sssaj1999.6351404x.

Walling D E, He Q, Appleby P G. 2002. Conversion Models for Use in Soil-Erosion, Soil-Redistribution and Sedimentation Investigations. Handbook for the Assessment of Soil Erosion and Sedimentation Using Environmental Radionuclides. Springer Netherlands, 111–159.

Walling D E, Porto P, Zhang Y, Du P. 2014. Upscaling the use of fallout radionuclides in soil erosion and sediment budget investigations: addressing the challenge. International Soil and Water Conservation Research, 2(3): 1-21. DOI: 10.1016/S2095-6339(15)30019-8.

Wu Y H, Li W, Zhou J, Cao Y. 2013. Temperature and precipitation variations at two meteorological stations on eastern slope of Gongga Mountain, SW China in the past two decades. Journal of Mountain Science, 10(3): 370–377. DOI: 10.1007/s11629-013-2328-y.

Zhang X B. 2005. Discussion on interpretations of ^{137}Cs depth distribution profiles of lake deposits. Journal of Mountain Science, 23(3): 294-299 (in Chinese). DOI: 10.1007/s10971-005-6694-y.

Zhou J, Wu Y, Prietzel J, Bing H, Dong Y, & Sun S. 2013. Changes of soil phosphorus speciation along a 120-year soil chronosequence in the Hailuogou Glacier retreat area (Gongga Mountain, SW China). Geoderma, 195(3): 251-259. DOI: 10.1016/j.geoderma.2012.12.010.

Zhou J, Wu Y, Bing H, Yang Z, Wang J, & Sun H. 2016. Variations in soil phosphorus biogeochemistry across six vegetation types along an altitudinal gradient in SW China. Catena, 142:102-111. DOI: 10.1016/j.catena.2016.03.004.

Figure captions

Fig. 1. Location of the research area in the Hailuogou Glacier Valley and sampling sites

Fig. 2. Particle size depth distributions of moraine soils at the nine sampling sites

Fig. 3. ^{137}Cs depth distributions in the soils at each of the moraine sampling sites

Fig. 4. $^{210}Pb_{ex}$ depth distributions in the soils at the nine moraine sampling sites

Fig.5. Exponential relationship between $^{210}Pb_{ex}$ inventories and the span times between the ages of the moraine deposited after glacier retreat and the sampling year

Table 1. Locations and glacier retreat times for the sampling sites

Sites	Retreat time	Latitude north	Longitude east	Altitude (m)	Distance from 2017's glacier toe (m)
R1	1990	29°34′05″	101°59′23″	2950	350
R2	1983	29°34′07″	101°59′44″	2938	510
R3	1972	29°34′13″	101°59′49″	2935	810
R4	1966	29°34′16″	101°59′54″	2945	1030
R5	1958	29°34′21″	102°00′03″	2925	1213
R6	1945	29°34′28.2″	102°00′18.5″	2934	1570
R7	1930	29°34′30.9″	102°00′23.7″	2913	1770
R8	1915	29°34′33.8″	102°00′28″	2890	2016
R9	1910	29°34′35.2″	102°00′32.4″	2832	2100

Table 2. ^{137}Cs and $^{210}Pb_{ex}$ inventories in soils at the nine moraine sampling sites.

Sites (glacier retreat time)	R1 (1990)	R2 (1983)	R3 (1972)	R4 (1966)	R5 (1958)	R6 (1945)	R7 (1930)	R8 (1915)	R9 (1910)
^{137}Cs inventory (Bq/m^2)	17.28	30.63	105.07	9.29	151.77	588.24	891.23	764.73	818.91
Errors	15.3	25.1	17.4	8.5	46.3	39.8	54.3	29.8	50.1
$^{210}Pb_{ex}$ inventory (Bq/m^2)	3669.6	4180.4	2026.9	8341.2	6966.7	4710.7	8704.2	7359.2	10718.9
Errors	218.5	216	327.1	232	244.5	147.1	143.6	67.3	167.4

Table 3. The actual and modelled span times (n) between the age of the moraine deposit formed after glacier retreat and the sampling year.

sites	R1	R2	R3	R4	R5	R6	R7	R8	R9
Actual span times (year)	26	33	44	50	58	71	86	101	106
Modelled span times (year)	26.2	30.5	13.6	79.1	58.7	35.1	86	63.8	169.8

Fig. 1. Location of the research area in the Hailuogou Glacier Valley and sampling sites

Fig. 2. Particle size depth distributions of moraine soils at the nine sampling sites

Fig. 3. ^{137}Cs depth distributions in the soils at each of the moraine sampling sites

Fig. 4. $^{210}Pb_{ex}$ depth distributions in the soils at each of the moraine sampling sites

Fig.5. Exponential relationship between $^{210}Pb_{ex}$ inventories and the span times between the ages of the moraine deposited after glacier retreat and the sampling year


China
N
Qinghai-Tibet Plateau
Hailuogou
0 500 1,000 1,500 2,000 km
Hailuogou Watershed
N
Sampling sites
Elevation
High : 7447 m
Low : 1434 m
0 2.5 5 7.5 10 km
101°59'30"E
102°0'0"E
102°0'30"E
29°34'30"N
29°34'0"N
N
3300
3200
3000
2900
2800
3100
3400
3700
R1
R2
R3
R4
R5
R6
R7
R8
R9
Legend
Sampling sites
Contour line
0 250 500 750 1,000 m
R1
R2
R3
R4
R5
R6
R7
R8
R9
Valley
Valley floor
Glacier toe

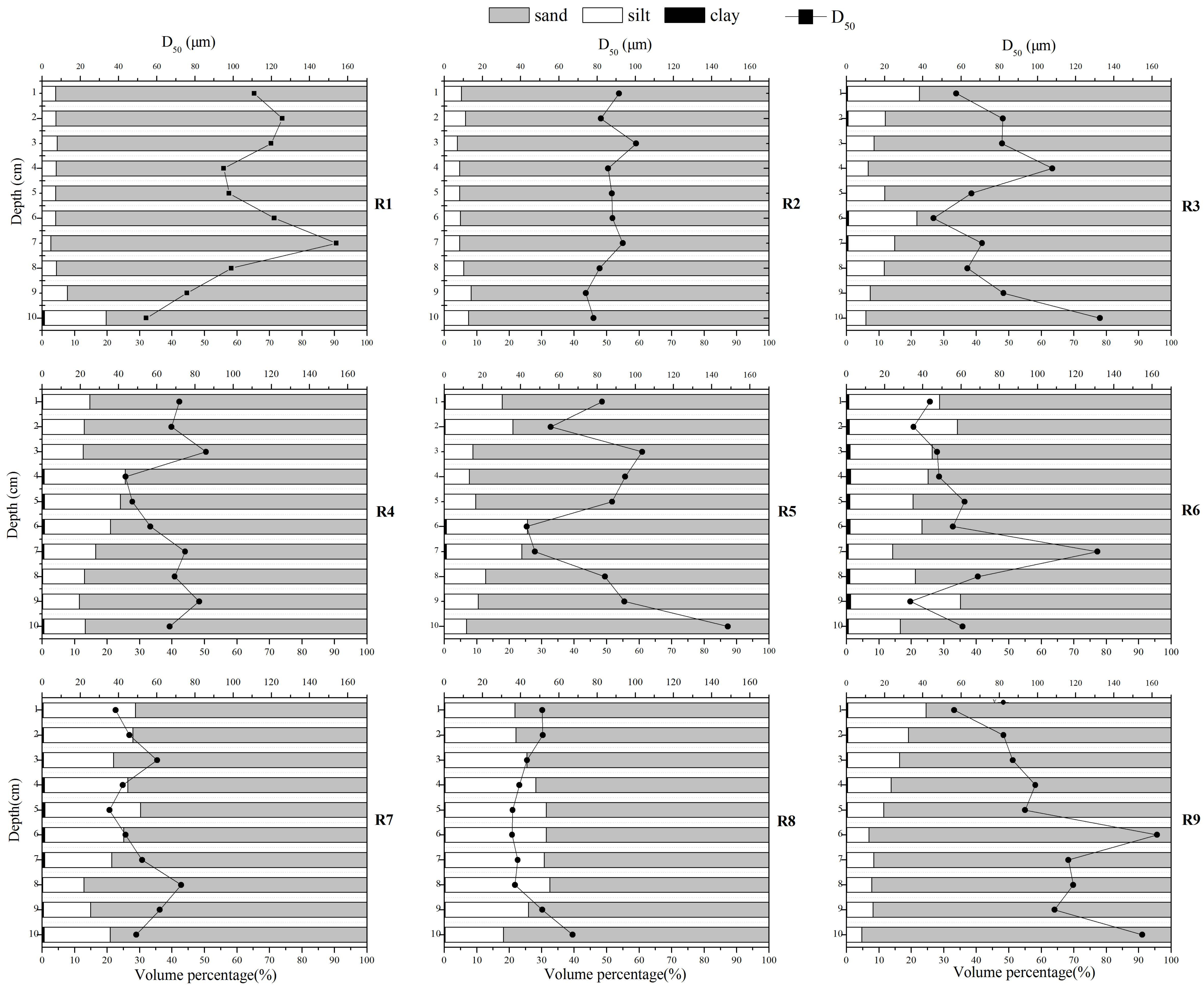
sand
silt
clay
D50
D50 (μm)
Depth (cm)
Depth(cm)
Volume percentage(%)
R1
R2
R3
R4
R5
R6
R7
R8
R9

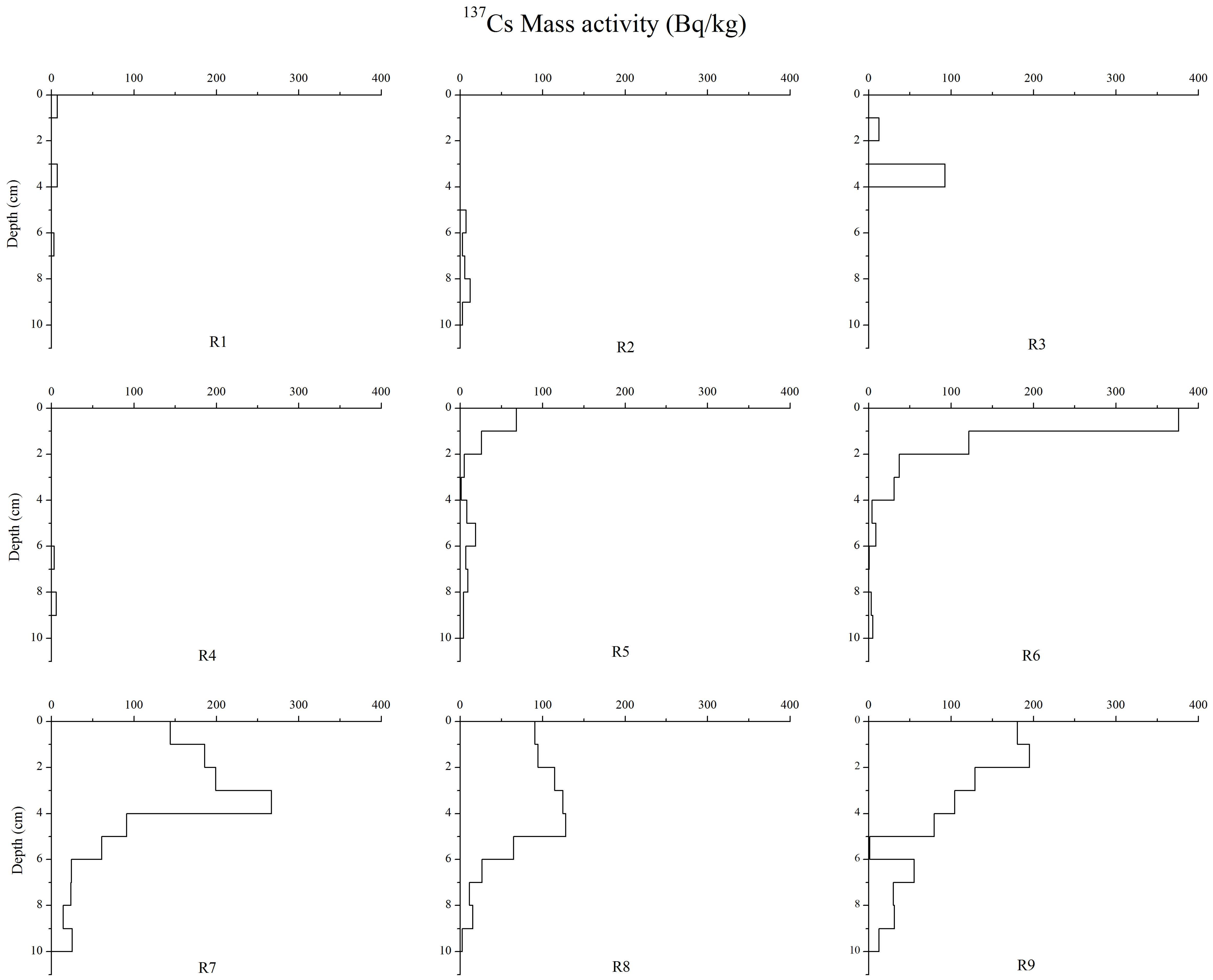

^{137}Cs Mass activity (Bq/kg)
Depth (cm)
0
100
200
300
400
0
2
4
6
8
10
R1
R2
R3
R4
R5
R6
R7
R8
R9

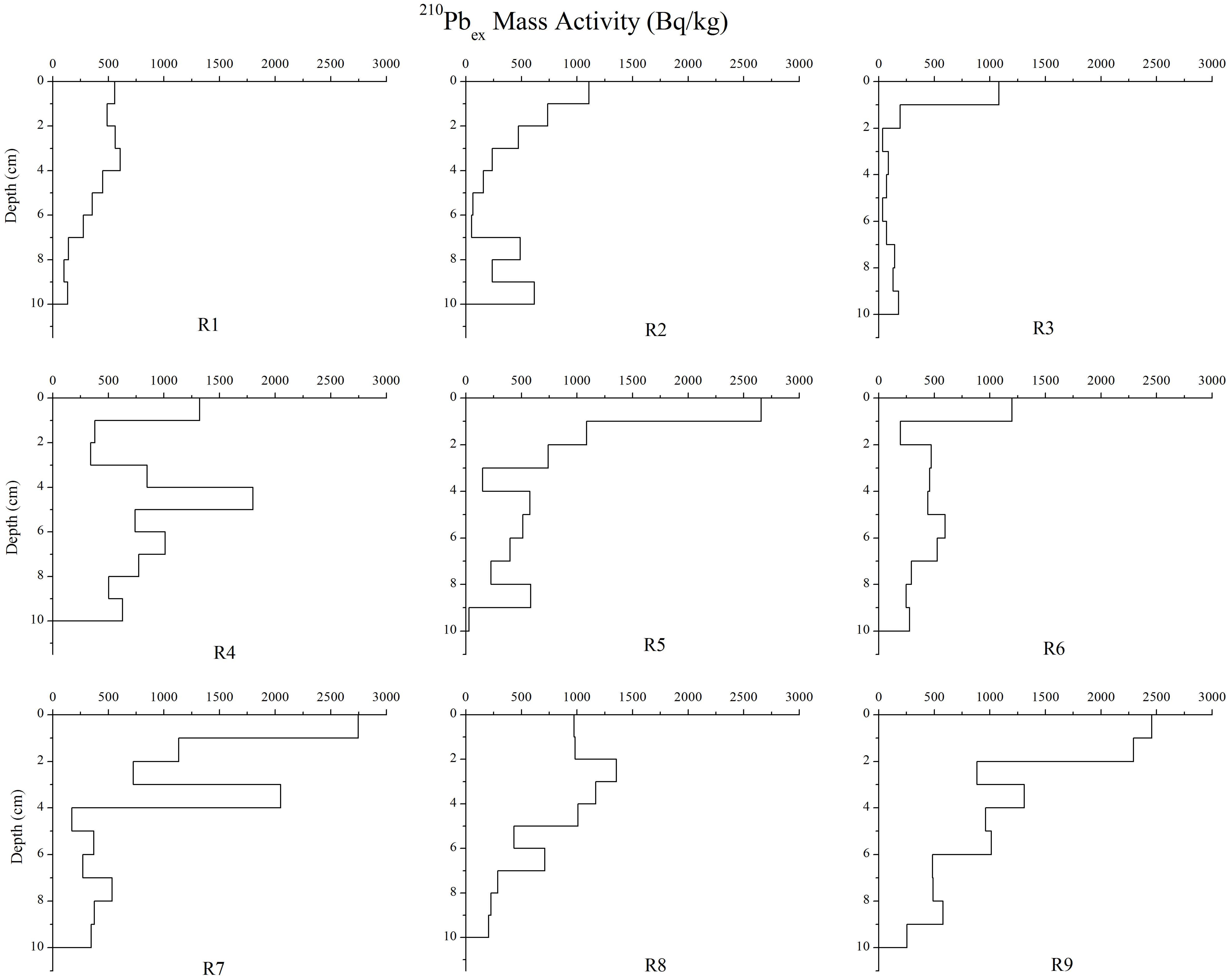

$^{210}Pb_{ex}$ Mass Activity (Bq/kg)
0
500
1000
1500
2000
2500
3000
Depth (cm)
0
2
4
6
8
10
R1
R2
R3
R4
R5
R6
R7
R8
R9

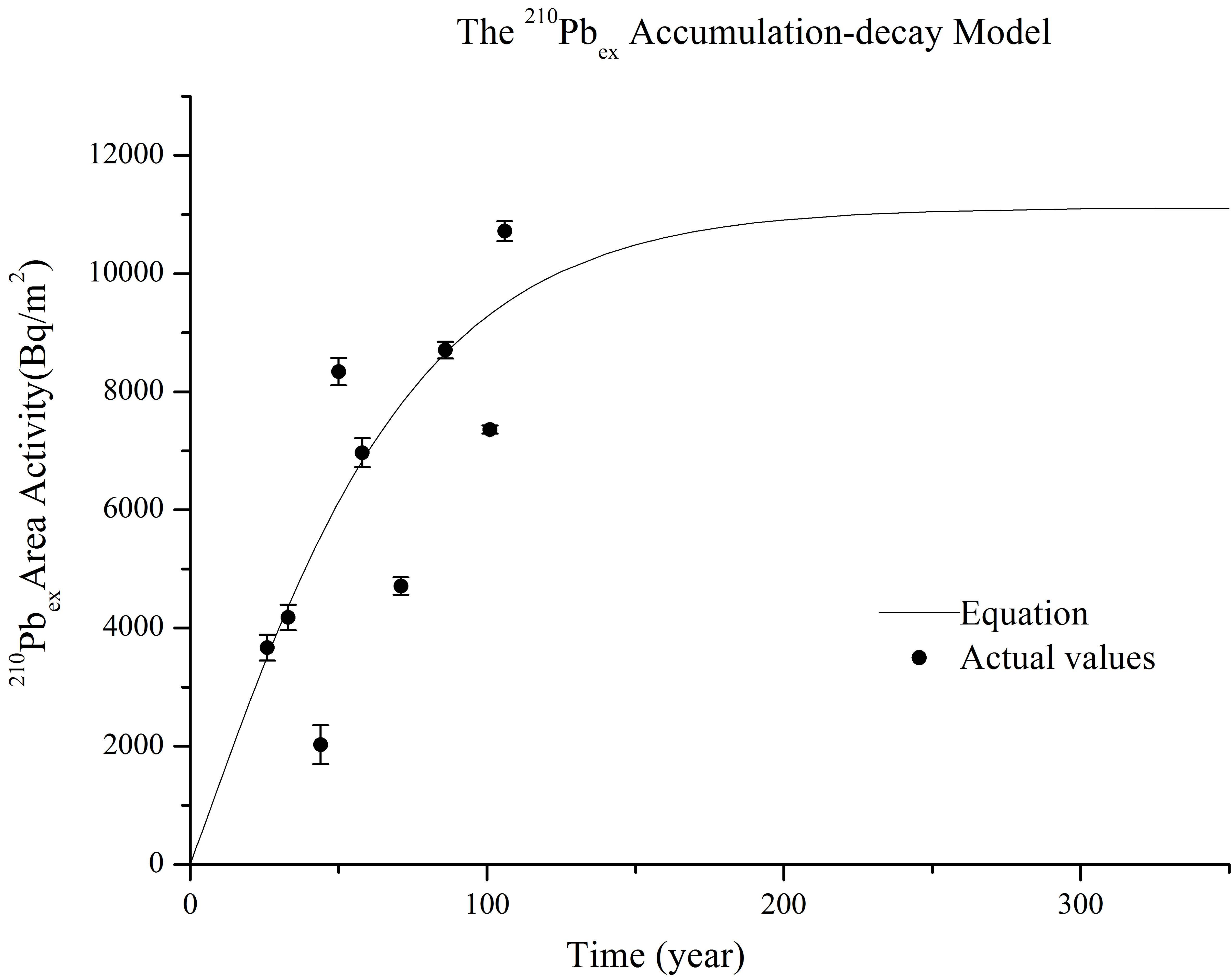

The $^{210}Pb_{ex}$ Accumulation-decay Model
$^{210}Pb_{ex}$ Area Activity(Bq/m^2)
0
2000
4000
6000
8000
10000
12000
0
100
200
300
Time (year)
Equation
Actual values